



# 1 Large-scale drivers of Caucasus climate variability in meteorological 2 records and Mt Elbrus ice cores

3  
4 Anna Kozachek<sup>1,2,3</sup>, Vladimir Mikhaleiko<sup>2</sup>, Valérie Masson-Delmotte<sup>3</sup>, Alexey Ekaykin<sup>1,4</sup>, Patrick  
5 Ginot<sup>5,6</sup>, Stanislav Kutuzov<sup>2</sup>, Michel Legrand<sup>5</sup>, Vladimir Lipenkov<sup>1</sup>, Susanne Preunkert<sup>5</sup>

6  
7 1. Climate and Environmental Research Laboratory, Arctic and Antarctic Research Institute, Saint Petersburg, 199397,  
8 Russia

9 2. Institute of Geography, Russian Academy of Sciences, Moscow, 119017, Russia

10 3. Laboratoire des Sciences du Climat et de l'Environnement, CEA/CNRS/UVSQ/IPSL, Gif-sur-Yvette, 91191, France

11 4. Institute of Earth Sciences, Saint Petersburg State University, Saint Petersburg, 199178, Russia

12 5. Laboratoire de Glaciologie et Géophysique de l'Environnement, CNRS/UGA, Grenoble, 38400, France

13 6. Observatoire des Sciences de l'Univers de Grenoble, IRD/UGA/CNRS, Grenoble, 38400, France

14  
15 *Correspondence to:* Anna Kozachek (kozachek@aari.ru)

## 16 17 **Abstract**

18  
19 A 181.8 m ice core was recovered from a borehole drilled into bedrock on the western plateau of Mt. Elbrus (43°20'53.9''  
20 N, 42°25'36.0'' E; 5115 m a.s.l.) in the Caucasus, Russia, in 2009 (Mikhaleiko et al., 2015). Here, we report on the results of  
21 the water stable isotope composition from this ice core in comparison with results from shallow ice cores. There is a distinct  
22 seasonal cycle of the isotopic composition which allowed dating by annual layer counting. Dating has been performed for  
23 the upper 126 m of the deep core combined with shallow cores data. The whole record covers one century from 2013 back to  
24 1914. Due to the high accumulation rate (1380 mm w.e. per year) and limited melting we obtained the isotopic composition  
25 and accumulation rate records with seasonal resolution. These values were compared with available meteorological data  
26 from 13 weather stations in the region, and also with atmosphere circulation indices, back-trajectories calculations and GNIP  
27 data in order to decipher the drivers of accumulation and ice core isotopic composition in the Caucasus region. In the  
28 summer season the isotopic composition depends on the local temperature, while in winter, the atmospheric circulation is the  
29 predominant driver of the ice core isotopic composition. The snow accumulation rate correlates well with the precipitation  
30 rate in the region all year round, this made it possible to reconstruct and expand the precipitation record at the Caucasus  
31 highlands from 1914 till 1966 when the reliable meteorological observations of precipitation at high elevation began.

## 32 33 **1 Introduction**

34  
35 Large scale modes of variability such as the NAO (North Atlantic Oscillation) and AMO (Atlantic Multidecadal Oscillation)  
36 are known to influence European climate variability (see review in Panagiotopoulos et al., 2002). However, most studies of



37 large-scale drivers of European climate change have been focused on low elevation instrumental records from weather  
38 stations, and there is very limited information about climate variability at high altitudes, and about differences in climate  
39 variability and trends at different elevations (EDW research group, 2015). Such differences were calculated in many  
40 mountain regions (EDW research group, 2015), except for the Caucasus, due to the lack of high elevation instrumental  
41 observations in this region.

42 The Caucasus is located southwards of the East European Plain. It is a high mountain region, with typical elevations of 3200-  
43 3500 m a.s.l., and with the highest point reaching 5642 m for Elbrus. The Main Caucasus Ridge acts as a barrier between  
44 subtropical and temperate mid-latitude climates, as observed for other high mountain regions such as the Himalaya. As in  
45 other mountain regions, there is a lack of high elevation meteorological records in the Caucasus. Moreover, existing records  
46 are relatively short: for example, reliable Caucasus precipitation measurements started only in 1966. An improved spatio-  
47 temporal coverage is required to investigate internal variability, to explore trends and spatial differences, and to evaluate the  
48 skills of atmospheric models providing atmospheric analysis products where no meteorological data are assimilated.

49 Measurements of the stable isotope composition of water, and annual accumulation rates in mid to high latitude ice cores are  
50 widely used proxies to estimate past temperature and precipitation rate changes. In many high mountain regions such as the  
51 Caucasus, and for elevations situated above the tree line, ice core data provides the only source of detailed information to  
52 document past climate changes, complementing punctual information retrieved from changes in glacier extent and recent  
53 glacier mass balance. For example study of the water stable isotope composition of several ice cores obtained in the Alps  
54 was recently conducted by Mariani et al. (2014) and the same research in Alaska was performed by Tsushima et al. (2015).  
55 The authors explored the links between the ice cores isotopic composition, local climate and large-scale circulation patterns.  
56 They found that in mountain regions isotopic composition of the ice cores governed both by the local meteorological  
57 conditions and by the regional and global factors. However, ice core records are complex. For instance, even in areas without  
58 any seasonal melt, accumulation is the net effect of precipitation, sublimation, and wind erosion processes, and may  
59 significantly differ from precipitation. Water stable isotope records are in mid to high latitudes physically related to  
60 condensation temperature through distillation processes, but the climate signal is archived through the snowfall deposition  
61 and post-deposition processes. One important artefact lies in the intermittency of precipitation, and the covariance between  
62 condensation temperature and precipitation, which may bias the climate record towards one season, or towards one particular  
63 weather regime, challenging an interpretation in terms of annual mean temperature. The water isotope content is more  
64 sensitive to distortion because of seasonality than the other ice core properties like aerosol concentration (Wagenbach et al.,  
65 2012). Moreover, water stable isotopes are integrated tracers of all phase changes occurring from evaporation to mountain  
66 condensation, and are also affected by non-local processes related to evaporation characteristics, or shifts in initial moisture  
67 sources. Such processes have the potential to alter the validity of an interpretation of the proxy record in terms of local,  
68 annual mean, or precipitation-weighted temperature. In some region, isotopic records are more related to hydrological  
69 cycles, recycling, rainout (Aemisegger et al., 2014). Finally, the condensation temperature may also strongly differ from  
70 surface air temperature, depending on elevation shifts in e.g. planetary boundary layer or convective activity (see Ekaykin



71 and Lipenkov, 2009 for a review). While these processes make the interpretation of ice core records complex, they  
72 conversely open the possibility that the ice core proxy record may be in fact more sensitive to large-scale climate variability  
73 than punctual precipitation amounts. For instance, Casado et al (2014) have evidenced a strong fingerprint of the NAO in  
74 water stable isotope records from central western Europe and Greenland, either in long instrumental records based on  
75 precipitation sampling, in seasonal ice core records, or in atmospheric models including water stable isotopes.

76 We will now briefly review earlier studies performed on climate variability in the Caucasus area, and which have already  
77 explored the relationships between regional climate, glacier expansion, and large-scale modes of variability: the NAO (North  
78 Atlantic Oscillation), AO (Arctic Oscillation), AMO (Atlantic Meridional Oscillation) and NCP (North Sea – Caspian  
79 Pattern). For example, Shahgedanova et al. (2005) monitored the mass balance of the Djankuat glacier, situated at an altitude  
80 between 2700 and 3900 m a.s.l. While no significant correlation was identified between accumulation rate and the winter  
81 NAO index, the years of high accumulation systematically occurred during winters with a very negative NAO index.  
82 Brunetti et al. (2011) explored the influence of the NCP mode on climate in Europe and around the Mediterranean region.  
83 They evidenced a negative correlation coefficient of -0.50 between temperature in the Caucasus and the NCP index. Baldini  
84 et al. (2008) investigated records of precipitation isotopic composition in Europe from the IAEA/GNIP stations,  
85 extrapolating a significant negative correlation between winter precipitation  $\delta^{18}\text{O}$  in the Caucasus region and the NAO index  
86 ( $R = -0.50$ ). Casado et al (2013) studied the influence of precipitation intermittency on the relationships between  
87 precipitation  $\delta^{18}\text{O}$ , temperature, and the NAO. The influence of the NAO index on European climate and precipitation  $\delta^{18}\text{O}$   
88 appeared more prominent in winter than in summer (Comas-Bru et al., 2016).

89 Here, we take advantage of the new Elbrus deep ice cores (Mikhalenko et al., 2015), and produce the first analysis of water  
90 stable isotope and accumulation records. Section 2 introduces the data and methods, with a description of the ice core  
91 analyses and age scale, an overview of regional meteorological information, as well as the source of information for indices  
92 of modes of variability. Section 3 presents the results of the comparison and statistical analyses of the relationships between  
93 regional climate parameters (temperature and precipitation), Elbrus ice core records, and modes of variability. In section 4,  
94 we finally summarize our key findings and the next steps envisaged to strengthen the climatic interpretation of the Caucasus  
95 ice core records.

## 96 **2 Data and methods**

### 99 **2.1 Ice core data**

#### 101 **2.1.1 Drilling site and drilling campaigns**

103 Here, we report on results from the new, deepest ice core from Mt Elbrus, in comparison with results from shallow ice cores.



104 Deep drilling was performed on the Western Plateau (43°20'53.9" N, 42°25'36.0" E; 5115 m a.s.l.) of Mt Elbrus (fig. 1) in  
105 September 2009, allowing recovery of a 181.8 m long ice core, down to bedrock. The drilling site and the drilling operations  
106 are thoroughly described in Mikhalenko et al. (2015).

107 In order to update the ice core records towards the present-day, and enable a comparison of the measurements with local  
108 meteorological monitoring data, surface drilling operations were repeated at the same place in 2012 (11.5 m long) and in  
109 2013 (20.5 m long). Results are also compared here with previously published isotopic composition data measured along the  
110 22 m shallow ice core drilled at the same place in 2004 which covered the period from 1998 till 2004. (Mikhalenko et al,  
111 2005).

112 In 2014, drilling operations were also successful at the Maili Plateau (Mt. Kazbek), at the altitude of 4500 m a.s.l. in 200 km  
113 eastwards from Elbrus (fig. 1), delivering a 20-m ice core. The Kazbek core is shown for the comparison only. Its detailed  
114 description will be published elsewhere.

115

### 116 2.1.2 Sampling process and sampling resolution

117

118 For the upper and the lower parts of the deep core (0-106 m and 158-181.8 m) and for the shallow firn cores drilled in 2012  
119 and 2013, sampling was performed using classical cutting-melting procedures. For the other depth intervals, melted samples  
120 were extracted from the continuous flow analysis system of LGGE (Grenoble, France), automatically sub-sampled, frozen  
121 and stored in vials for subsequent isotopic analysis. The description of the CFA system will be published elsewhere.

122 The sampling resolution was 15 cm for the upper 16 m of the deep core (see the sketch of the sampling resolution in fig. 2c).  
123 It was then increased to 5 cm in order to achieve better resolution, from 16 to 70 m depth and in the bottom part of the core  
124 (158-182 m depth). To ensure 15-20 samples per year, the sampling resolution was increased to 4 cm in the depth range from  
125 70 to 106 m, similar to the sampling resolution of the CFA system (3.7 cm).

126 Samples from the shallow cores drilled in 2012 and 2013 were cut with a resolution of 10 and 5 cm, respectively.

127

### 128 2.1.3 Isotopic measurements

129

130 Water stable isotope ratios ( $\delta^{18}\text{O}$  and  $\delta\text{D}$ ) were measured at the Climate and Environmental Research Laboratory (CERL) of  
131 Arctic and Antarctic research Institute (St Petersburg, Russia), using a Picarro L2120-i analyzer. Each sample was measured  
132 once. Sequences of measurements included the injection of 5 samples, followed by the injection of an internal laboratory  
133 standard with an isotopic value close to that of the samples. We also repeated the measurements of about 10% of all the  
134 samples in order to calculate the analytical precision: 0.06‰ for  $\delta^{18}\text{O}$  and 0.30‰ for  $\delta\text{D}$ . The depth profile of  $\delta^{18}\text{O}$   
135 (Mikhalenko et al., 2015; Kozachek et al., 2015) and of the deuterium excess ( $d = \delta\text{D} - 8 * \delta^{18}\text{O}$ ) are shown in fig. 2.

136 Moreover, 600 samples from the depth interval from 23 to 35 m were measured in the Laboratory of Isotope Hydrology of  
137 the IAEA (Vienna, Austria). The two records are highly correlated ( $r=0.99$ ,  $p < 0.05$ ) for both isotopes (Figure S2b) with a



138 systematic offset of 0.2 ‰ for  $\delta^{18}\text{O}$  and 1 ‰ for  $\delta\text{D}$ . The records of the second order parameter deuterium excess are also  
139 significantly correlated ( $r=0.65$ ,  $p < 0.05$ ) without any specific trend or systematic offset. This inter-laboratory comparison  
140 demonstrates the high quality of the isotopic measurements performed in CERL.

141 We also stress the close overlap of the upper part of the profiles of the water stable isotope records versus depth from the  
142 different cores drilled in 2009, 2012 and 2013 (Fig. S2a). Based on this close agreement within the different shallow firn  
143 cores, we decided to calculate a stack record for the period from 1914 till 2013 which is used hereafter for the dating.

144 In the depth interval from 100 to 106 m depth, we also have an overlap of samples obtained with classical cutting method  
145 and CFA method described above, without any significant difference (Fig. S2c), again allowing us to combine the two  
146 records into one stack record.

147

#### 148 2.1.4 Dating

149

150 The chronology is based on the identification of annual layers. These are prominent in  $\delta^{18}\text{O}$  with the average seasonal  
151 amplitude of 20 ‰. We used the mean value of the  $\delta^{18}\text{O}$  of the whole dataset (-15.5 ‰) as a threshold to separate between  
152 the warm and cold seasons. For equivocal situations, we also used additional data: melt layers and dust layers (used to  
153 identify the warm season) (Kutuzov et al., 2013) as well as ammonium and succinic acid concentration data that also have  
154 seasonal variations (Mikhalenko et al., 2015). We compared annual layers counting performed independently using the  
155 seasonal cycles in the isotopic composition and the ammonium concentration. The discrepancy between two independent  
156 chronologies is  $\pm 1$  year at a depth of 126 m. Hereafter, we focus our analysis on one century, from 1914 till 2013, which  
157 corresponds to the upper 126 m of the core. This period has been chosen because of relatively small dating uncertainty ( $\pm 1$   
158 year) and the availability of other records such as local meteorological observations. Figure 3 illustrates the identification of  
159 years. For a detailed description of the raw isotopic data and annual layers allocation for the upper 106 m of the core, please  
160 refer to Mikhalenko et al. (2015). Mean seasonal values of  $\delta^{18}\text{O}$  and  $d$  obtained as a result of the dating are shown in fig. 5  
161 and 6 respectively.

162 The annual accumulation rate is calculated as the thickness of the seasonal layer, multiplied by the layer density using the  
163 density profile from Mikhalenko et al. (2015), and corrected for layer thinning using the Dansgaard-Johnsen model  
164 (Dansgaard and Johnsen, 1969), with the following parameters: accumulation rate 1.583 m of ice equivalent, pore close-off  
165 depth = 55 m (Mikhalenko et al., 2015).

166

#### 167 2.1.5 Diffusion of stable isotopes

168

169 We calculated the potential influence of diffusion on the stable isotopes record according to (Johnsen, 2000) model. Our  
170 calculation showed that the seasonal amplitude of  $\delta^{18}\text{O}$  variations could be 10-20% less because of the diffusion. If it was the  
171 case we would observe a decreasing of  $\delta^{18}\text{O}$  maxima and increasing of minima with depth. Moreover we would find a



172 positive correlation between accumulation rate and seasonal amplitude of  $\delta^{18}\text{O}$ . These features have not been found in the ice  
173 core data. We therefore consider that the diffusion does not influence sufficiently the isotopic composition record in the  
174 upper 126 m of the ice core. At the bottom part of the core (e.g. at a depth of 180 m) the annual cycle of  $\delta^{18}\text{O}$  should have an  
175 amplitude of 4 ‰ which is detectable but the length of the cycle should be less than 1 cm. Thus, for obtaining climatic  
176 information from the bottom part of the core very high sampling resolution is required.

## 178 2.2 Meteorological data

179  
180 We used the daily meteorological data (precipitation rate and mean daily temperature) from several weather stations around  
181 the drilling site (see map in Fig. 1 and Table 1) for comparison with the ice core data. We also investigated records of  
182 precipitation isotopic composition based on monthly sampling, performed at three stations to the south of Caucasus within  
183 the WMO-IAEA Global Network of Isotopes in Precipitation (GNIP) program (Table 1).

184 For comparison we used the NCEP/NCAR reanalysis temperature data (Kalnay et al., 1996) for the 500 mbar level which  
185 corresponds to the drilling site altitude. Two different models were used to calculate back trajectories: FLEXPART (Forster  
186 et al., 2007, Stohl et al., 2009), HYSPLIT (Draxler, 1999, Stein et al., 2015, Rolph, 2016). The LMDZiso model was used to  
187 estimate the precipitation isotopic composition at the drilling site (Risi et al., 2010).

## 189 3 Results

### 191 3.1 Regional climate

192  
193 The main peculiarity of the drilling site is its location on the border between subtropical and temperate climatic zones  
194 (Volodicheva, 2004). Back-trajectory calculations show that the drilling site is characterized by remarkable seasonal  
195 differences in moisture sources locations. In winter, the origin of air masses varies from the Mediterranean to the North  
196 Atlantic. In summer, local moisture sources from the surrounding continents or from the Black Sea are predominant (see fig.  
197 S1 for examples).

198 Meteorological data depict large regional variations in the seasonal cycle of precipitation. To the south of the Caucasus, there  
199 is no distinct seasonal cycle (Fig. 4a), showing the climatology for the Klukhorsky Pereval station. In fact, the Klukhorsky  
200 Pereval station is situated north of the Main ridge, but in terms of the seasonal cycle of precipitation it undoubtedly belongs  
201 to the southern group. But we are nevertheless using this station as an example because of the uninterrupted record of  
202 temperature and precipitation for the 1966-1990 period. By contrast, the north of the Caucasus is marked by a distinct  
203 seasonality in precipitation amounts, which are maximum in summer and minimum in winter (Fig. 4b), showing the  
204 climatology for the Mineralnye Vody station. Moreover, the annual precipitation rate to the south of the Caucasus is much  
205 higher than to the north. For example, the typical annual precipitation rate to the north of the Caucasus at the altitude close to





206 the sea level is 500 mm per year, while to the south of the Caucasus at the same altitude it is about 1500 mm. The amount of  
207 precipitation in the region is affected by the altitude and the distance from the sea shore.

208 The seasonal changes of temperature appear uniform all over the region surrounding Caucasus, with warmest conditions  
209 observed in summer and coldest conditions observed in winter. The seasonal amplitude depends on the distance from the sea  
210 and the mean annual temperature depends on the altitude. The average regional lapse rate was calculated using the available  
211 meteorological data. It is minimum in winter (2.3°C per 1000 m) and maximum (5.2 °C per 1000 m) in summer (Fig. S3).

212 Based on the coherency of temperature variability at all the weather stations in this region, we calculated a regional stack  
213 temperature record. Normalized temperature time series were calculated for each station for each season or for the whole  
214 year, and results were then averaged (see Fig. 8a and 8b for seasonal stack records). For precipitation data, available in this  
215 region since 1966, we considered two different stacks (fig. S4), separating the stations with a distinct seasonal cycle from  
216 those where no seasonal cycle was identified for precipitation rates. We coherently used the reference period from 1966 to  
217 1990 for normalization for both precipitation rate and temperature.

218 At our drilling site, an automatic weather station (AWS) provided in situ measurements for the period from August 2007 till  
219 January 2008. The day to day variations of temperature at low elevation weather stations and at the AWS are coherent for the  
220 whole period of the AWS work.

221 We also compared the data from meteorological stations with the NCEP reanalysis (Kalnay et al., 1996) outputs (not shown)  
222 for the 500 mbar level. Despite difference in absolute values on the daily scale when compared with the AWS data (the  
223 difference is random and varies from -1 to 1 °C), the observed regional data and reanalysis data have the same month to  
224 month variability. The maximum daily mean temperature at the drilling site according to the reanalysis data was -1.3 °C for  
225 the whole dataset. The temperature in the glacier at 10m depth, which correspond to the annual mean temperature at the  
226 drilling altitude, is -17 °C (Mikhaleenko et al., 2015), the annual mean temperature at the drilling altitude from the NCEP  
227 reanalysis is -14 °C, and the same value calculated from meteorological observations and corrected for the lapse rate is -11  
228 °C.

229 Hereafter in the meteorological data, we considered the cold season or winter of a given year to range from November of the  
230 previous year till April of the current year, and the warm season or summer from May till October.

231 We then investigated long-term trends in the composite meteorological records. It is evident that last 20 years in summer  
232 season were the warmest for the whole observation period (fig. 8), while in winter the recent warming is not unprecedented.  
233 For example, winters in the 1960s – 1970s were even warmer (fig. 8). Multi-decadal patterns of temperature variations also  
234 differ in the late 19<sup>th</sup> Century, where negative anomalies are identified in winter temperature (Fig. 8) but not in summer  
235 temperature (Fig 8). On the other hand in winter temperatures we can observe lower temperatures at the end of 19<sup>th</sup> century  
236 that can be impact of the volcanic eruptions (Stoffel et al., 2015). We also noted the high temperature values in the 1910s -  
237 1920s that is not completely understood. We did not find any trends in the precipitation rate for neither of the groups of  
238 stations (fig. S4).



239 A significant anti-correlation is observed between temperature and the NAO index, both in winter and summer (Table 2, the  
240 information about the time series used for the correlation analysis can be found in Table 1). Stronger anti-correlations are  
241 identified between temperature and the NCP index, especially in winter, as also reported by Brunetti et al. (2011). A weak  
242 positive correlation is identified between AMO and summer temperature. Relationships with indices of large scale modes of  
243 variability are systematically weaker for precipitation, with contradictory results for the south/north Caucasus stack; they  
244 appear significant for the NCP in summer and winter (Table 2).

245 GNIP data are only available at low elevation stations. They show a rather uniform distribution of the isotopic composition  
246 of precipitation in the region during summer, as well as a gradual depletion of  $\delta^{18}\text{O}$  at higher altitudes in winter.

247 GNIP records are too short and intermittent (one-two years with gaps) to investigate the variability and relationships with the  
248 local temperature on interannual scale. We therefore restrict discussion of GNIP data to seasonal variations. The  $\delta^{18}\text{O}$  and  $\delta\text{D}$   
249 in precipitation have a distinct seasonal cycle with maximum values observed in warm season (JJA) and minimum values  
250 observed in cold season (DJF). As an example we show the seasonal cycle of  $\delta^{18}\text{O}$  and  $d$  for Bakuriani station in 2009 (fig.  
251 7). This station is the only one in the region for which the whole uninterrupted dataset for one annual cycle is available. The  
252 seasonal amplitude of  $\delta^{18}\text{O}$  is about 10 ‰. The  $d$  variations show no seasonal cycle varying randomly between 10 ‰ and 25  
253 ‰. We found no significant correlation between  $\delta^{18}\text{O}$  and  $d$ .

254 Climate variability as a driver for glacier variations in the Caucasus has recently been explored by several authors.  
255 Elizbarashvili et al. (2013) found the increased frequency of extremely hot months during the 20th century, especially over  
256 Eastern Georgia, whereas number of extremely cold months decreased faster in the Eastern than in the Western region. In  
257 addition, highest rates for positive trends of annual mean air temperature can be observed in the Caucasus Mountains.  
258 Shahgedanova et al. (2014) evidenced significant glacier recession at the northern slopes of the Caucasus, consistent with  
259 increasing air temperature of the ablation season. They report that the most recent decade (2001-2010) was 0.7 – 0.8 °C  
260 warmer than in 1960-1986 at Terskol and Klukhorskij Pereval stations (see Table 1 for information on stations). However,  
261 the warmest decade for JJA was 1951-1960 (Shahgedanova et al., 2014). Tielidze (2016) reports recent increase of the  
262 annual mean temperatures at different elevations in the Georgian Caucasus. The region experienced glacier area loss over the  
263 20<sup>th</sup> century at an average annual rate of 0.4% with a higher rate in eastern Caucasus than in the central and western sections.  
264 The analysis of temperature and radiation regime of glaciers at the ablation period has been performed at Elbrus vicinities  
265 recently (Toropov et al., 2016). The authors prove that the observed waning of glaciers can not be explained by increase of  
266 temperature during the ablation period because of increase of precipitation during the accumulation period. They concluded  
267 that the main driver of glacier retreat is increase of the solar radiation balance for 4% for the 2001-2010 period which  
268 corresponds to increase of ablation for 140 mm per ablation season (Toropov et al., 2016).

269

### 270 3.2 Ice core records

271





272 The comparison of the four cores obtained at the Western Plateau of Elbrus shows similar variations during overlap periods  
273 (see Fig. 2S). We therefore calculate a stack record for each season, based on the average value of individual ice cores for the  
274 overlapping seasons. The inter-core disagreement is almost negligible (fig. 2S) and can be explained by different sampling  
275 resolution.

276 We note that the shallow ice core from the Maili plateau of Kazbek shows the same mean values of  $\delta^{18}\text{O}$  as the Elbrus ice  
277 cores during their overlap period. This is a surprise, given the difference in elevation (500 m) and continentality (200 km  
278 distance).

279 The inter-annual variability in isotopic composition is about twice larger in winter than in summer for  $\delta^{18}\text{O}$ . Different  
280 patterns of inter-annual to multi-decadal variations appear in the instrumental temperature data (see section 3.1) and ice core  
281  $\delta^{18}\text{O}$  records (Fig 5) emerge for winter versus summer. Consequently, we do not investigate annual mean results, and focus  
282 on each season.

283 The  $\delta\text{D}$  and  $\delta^{18}\text{O}$  values are highly correlated ( $r = 0.99$ ) on sample to sample scale so hereafter we use the  $\delta^{18}\text{O}$  information  
284 for the dating and comparison with the other parameters. The slope between  $\delta^{18}\text{O}$  and  $\delta\text{D}$  is 8.03 on sample to sample scale  
285 and 7.9 on seasonal scale without any significant difference between the two seasons.

286 No significant (R squared is insignificant at  $p < 0.05$ ) centennial trend is identified in winter / summer  $\delta^{18}\text{O}$ , nor in winter /  
287 summer accumulation rate or deuterium excess. We observe large variations in  $\delta^{18}\text{O}$  with high and variable values early 20<sup>th</sup>  
288 century, lower and more stable values in the 1940s-1960s, and a step increase in the 1970s with another level. These  
289 variations are coherent in both seasons but are not reflected in the meteorological observations. There is also an increase of  
290  $\delta^{18}\text{O}$  in the last two decades in both seasons in regard to the 1970s-1980s values but the absolute values of  $\delta^{18}\text{O}$  are close to  
291 the multiannual seasonal averages (Table 3). The highest decadal values of  $\delta^{18}\text{O}$  in both summer and winter are observed in  
292 1912-1920. While a recent warming trend is observed in the regional meteorological data (in summer), it is much less  
293 prominent in the ice core  $\delta^{18}\text{O}$  record, suggesting a divergence between  $\delta^{18}\text{O}$  and regional temperature. One of the possible  
294 explanations for this feature is the post-depositional change of the isotopic composition. But we do not expect a significant  
295 influence of the post-depositional processes because of high snow accumulation rate. The highest  $\delta^{18}\text{O}$  values for a single  
296 year correspond to the summer periods of 1984 and 1928, two years for which no unusual feature is identified from  
297 meteorological observations. The highest snow accumulation rate (fig. 9) is observed in both seasons of 2010, in coherence  
298 with the meteorological precipitation data, and also corresponding with a record low winter NAO index.

299 Our deuterium excess record (fig. 2b) does not depict any robust seasonal variation. Moreover, the distribution of deuterium  
300 excess as a function of  $\delta^{18}\text{O}$  does not display any clear structure. By contrast, deuterium excess is weakly positively  
301 correlated with the accumulation rate during summer ( $r = 0.27$ ,  $p < 0.05$ ). This finding is consistent with the GNIP data in the  
302 region that show no link between  $\delta^{18}\text{O}$  and deuterium excess. The smoothed values of deuterium excess have prominent  
303 cycles with a period of about 25 years that are synchronous in both seasons (fig. 6). Deuterium excess is highly sensitive to  
304 surface humidity, which itself is very different and depends on the arrival of maritime air masses or dry continental air  
305 masses. This may add to the complexity of the deuterium excess signal (Pfahl and Wernli, 2008).



306

307 **3.3 Comparison of ice core records with regional meteorological data**

308

309 We compared the ice core data with the regional meteorological data and the large scale modes of variability. The result of  
310 the correlation analysis is summarized in Table 4. Multiannual variations of the parameters are shown in fig. 9 for the winter  
311 period and in fig. 10 for the summer period.

312 We found no significant correlation between the ice core  $\delta^{18}\text{O}$  record and regional temperature, neither with the reanalysis  
313 data, nor with the observation data, when using the whole period. A significant correlation ( $r = 0.52$ ,  $p < 0.05$ ) emerges for  
314 summer data, when calculated for the period since 1984. The slope for this period is 0.25 per mille per  $^{\circ}\text{C}$ . We also repeated  
315 our linear correlation analysis using precipitation weighted temperature, and obtained the same results. This result implies  
316 that the isotopic composition at Elbrus is controlled by both local and regional factors such as changes in moisture sources.  
317 The possibilities for accurate reconstructions of past temperatures are therefore limited. For more accurate investigation of  
318 the  $\delta^{18}\text{O}$  – temperature relation on-site experiments and subsequent modelling is required. Our results are comparable to  
319 those obtained in the Alps by Mariani et al. (2014): again, while the seasonal cycle of ice core  $\delta^{18}\text{O}$  appears related to that of  
320 temperature, this is not the case for inter-annual variations, driven by other factors such as changes in moisture sources.  
321 Another research performed in the Alps by (Bohleber et al., 2013) revealed significant correlation of modified local  
322 temperature and the ice core isotopic composition at decadal scale. The authors also report that there are some periods of  
323 correlation absence. The main finding is that for the periods of less than 25 years the difference between the modified  
324 according to the authors' method and original dataset temperature is crucial but for longer periods the two temperature  
325 datasets are close to each other. That conclusion implies that the isotopic composition reflects the local temperature in the  
326 high mountain regions to a limited extent. It seems to be impossible to calculate the modified temperature for the Caucasus  
327 region according to the methods described by (Bohleber et al., 2013) because of the relatively short and sparse original  
328 datasets.

329 We also compared the annual mean temperatures and  $\delta^{18}\text{O}$  values disregarding the difference in the isotopic composition  
330 trends in different seasons. The regression analysis showed significant negative correlation between the two parameters. The  
331 regression equation for 11-year running means in the 1914-1928 and 1994-2013 differs from the same for the 1929-1993  
332 (see fig. 11 for the correlation plot and regression equations). The shifts can be explained by a sharp change of the climatic  
333 system. The negative correlation between  $\delta^{18}\text{O}$  and local temperature has already been observed in Antarctica (Vladimirova  
334 and Ekaykin, 2014). It can be explained by the change of the moisture source that can lead to increase of the difference  
335 between the source temperature and local temperature while local temperature slightly decreases.

336 Seasonal accumulation rate is linked to the precipitation rate on the stations situated south of the Caucasus in both seasons  
337 ( $r = 0.45$ ), and even more closely related to precipitation from Klukhorski Pereval station ( $r = 0.65$  for both seasons). We  
338 therefore establish a linear regression model for the period 1966-2013, and use this methodology to reconstruct past  
339 precipitation rates (1914-1965), when meteorological records are not reliable or not available. The reconstructed records are



340 shown on fig. 9 and 10 for the winter and summer seasons respectively. We found no significant trend in the reconstructed  
341 precipitation values. Even so, these results can be useful for validation of regional climate models and water resource  
342 assesment.

343 Calculation of the seasonal cycle of precipitation isotopic composition using the LMDZiso model (Risi et al., 2010) do not  
344 correspond to the results obtained from the ice core in absolute values or in amplitude. This can be explained by a  
345 complicated relief of the region that influences strongly the isotopic composition, but it is not taken into account in the  
346 model. Also in summer Elbrus is in a local convective precipitation system that is not included in the model.

347

### 348 **3.4 Comparison of ice core records with large scale modes of variability**

349

350 We report a significant ( $p < 0.05$ ) negative correlation ( $r = -0.33$ ) between the ice core accumulation rate record and NAO in  
351 winter. Moreover, the year of extremely high accumulation in both seasons (2010) coincides with an extremely low NAO  
352 winter index. The role of NAO in regional climate had also been evidenced by Shahgedanova et al. (2005) for the mass-  
353 balance of the Djankuat glacier situated in 30 km south-east of Elbrus for the period of 1967-2001. Interestingly, the  
354 accumulation record is related to the variability of regional precipitation, but the latter is not significantly related to the  
355 NAO. This may suggest different influences of large-scale atmospheric circulation on precipitation at lower versus higher  
356 elevations.

357 The ice core winter  $\delta^{18}\text{O}$  record shows a positive correlation with the NAO index ( $r = 0.42$ ), while the NAO index is  
358 negatively correlated with regional temperature ( $r = -0.42$ ). It also contradicts the findings of Baldini et al (2008) who, based  
359 on the GNIP low elevation dataset, extrapolated a negative correlation between the  $\delta^{18}\text{O}$  of precipitation and the NAO in this  
360 region. This finding also suggests different drivers of temperature and  $\delta^{18}\text{O}$  at low and higher elevation. We propose the  
361 following explanation for this correlation. During the positive NAO phase, the predominant moisture source for the  
362 Caucasus precipitation is the Mediterranean. During the negative NAO phase the moisture source is the Atlantic. In the first  
363 case the precipitation  $\delta^{18}\text{O}$  preserved in the ice core is higher because of higher initial sea water isotopic composition (Gat et  
364 al., 1996) and shorter distillation pathway. In the opposite situation the initial water isotopic composition is close to 0 ‰  
365 (Frew et al., 2000) and the distillation pathway is longer which leads to lower values of precipitation  $\delta^{18}\text{O}$ .

366 In order to explore the relationships of the Elbrus ice core datasets with the AMO, we used 20-year smoothed data. We show  
367 a negative correlation between the AMO index and the summer ice core  $\delta^{18}\text{O}$  signal ( $r = -0.53$ ) and a positive correlation  
368 between the AMO index and the winter accumulation record ( $r = 0.52$ ). As the correlation analysis between the ice core data  
369 and AMO index was performed with smoothed records it is not reported in Table 4, in order to avoid misunderstanding.

370 We explored the links between the ice core parameters ( $\delta^{18}\text{O}$ , accumulation rate) with the NCP index and found no  
371 significant correlation neither in winter nor in summer despite the significant correlation between the NCP and local  
372 temperature and precipitation. A possible explanation may be that the NCP pattern only affects low elevation regional  
373 climate but not high elevation climate.



374 No significant correlation was identified between deuterium excess and indices of large scale modes of variability. So far, no  
375 regional or large-scale climate signal could be identified in Elbrus deuterium excess. Further investigations using  
376 backtrajectories and diagnoses of moisture source and evaporation characteristics will be needed to explore further the  
377 drivers of this second-order isotopic parameter.

378

#### 379 **4 Conclusion**

380

381 We found no persistent link between ice cores  $\delta^{18}\text{O}$  and temperature, common feature emerging from non-polar ice cores  
382 (e.g. Mariani et al., 2014). This finding is not an artifact of high elevation versus low elevation difference because the  
383 variability of the regional temperature stack used for this comparison is in good agreement with the variability of the  
384 temperature at the drilling site as observed by the local AWS.

385 Our ice core records depict large decadal variations in  $\delta^{18}\text{O}$  with high and variable values in the late 19<sup>th</sup> - early 20<sup>th</sup>  
386 centuries, lower and more stable values in the 1940s-1960s, followed by a step increase in the 1970s. No unusual recent  
387 change is detected in the isotopic composition or in the accumulation rate record, in contrast with the observed warming  
388 trend from regional meteorological data. The accumulation rate appears significantly related to the NAO index coherently  
389 with the earlier results for the Djankuat glacier (Shahgedanova et al. 2005).

390 Based on regional meteorological information and trajectory analyses, the main moisture source is situated not far from the  
391 drilling site in summer, and consists of evaporation from the Black Sea and continental evapotranspiration. Changes in  
392 regional temperature during summer may affect the initial vapour isotopic composition as well as the atmospheric distillation  
393 processes, including convective activity, in a complex way. This may explain the significant albeit non persistent correlation  
394 of summer  $\delta^{18}\text{O}$  and temperature. Winter moisture sources appear more variable geographically, with potential contributions  
395 from the North Atlantic to the Mediterranean regions. Changes in moisture origin appear to dominate in regional  
396 temperature-driven distillation processes. As a result, the ice core isotopic composition appears mostly related to  
397 characteristics of large-scale atmosphere circulation such as the NAO index. The changes in moisture origin also influence  
398 deuterium excess parameter, which does not have any prominent seasonal variations.

399 Our data can be used in atmospheric models equipped with water stable isotopes for instance in order to assess their ability  
400 to resolve NAO – water isotope relationships (Langebroek et al., 2011, Casado et al., 2014). The accumulation rate at the  
401 drilling site is highly correlated with the precipitation rate and gives information about precipitation variability before the  
402 beginning of meteorological observations.

403

#### 404 **Acknowledgements**

405

406 The research was supported by the RFBR grant 14-05-31102, the measurement of the samples in IAEA was conducted  
407 according to research contracts 16184\R0, and 16795. This research work was conducted in the framework of the



408 International Associated Laboratory (LIA) “Climate and Environments from Ice Archives” 2012–2016, linking several  
409 Russian and French laboratories and institutes. We thank Obbe Tuinenburg and Jean-Louis Bonne for the back trajectories  
410 calculations.

411

412 **References**

413 Aemisegger F., Pfahl S., Sodemann H., Lehner I., Seneviratne S.I., Wernli H.: Deuterium excess as a proxy for continental  
414 moisture recycling and plant transpiration, *Atmos. Chem. Phys.*, 14, 4029–4054, doi:10.5194/acp-14-4029-2014, 2014.

415 Baldini L.M., McDermott F., Foley A.M., Baldini J.U.L.: Spatial variability in the European winter precipitation  $\delta^{18}\text{O}$ -NAO  
416 relationship: Implications for reconstructing NAO-mode climate variability in the Holocene, *Geophys. Res. Letters*. 35,  
417 doi:10.1029/2007GL032027, L04709, 2008.

418 Bohleber P., Wagenbach D., Schoner W., Bohm R.: To what extent do water isotope record from low accumulation Alpine  
419 ice cores reproduce instrumental temperature series? *Tellus B*, 65, 20148, doi:10.3402/tellusb.v65i0.20148, 2013.

420 Brunetti M., Kutiel H.: The relevance of the North-Sea Caspian Pattern (NCP) in explaining temperature variability in  
421 Europe and the Mediterranean, *Nat. Hazards Earth Syst. Sci.*, 11, 2881–2888, doi:10.5194/nhess-11-2881-2011, 2011.

422 Casado M., Ortega P., Masson-Delmotte V., Risi C., Swingedouw D., Daux V., Genty D., Maignan F., Solomina O., Vinter  
423 B., Viovy N., Yiou P.: Impact of precipitation intermittency on NAO-temperature records, *Clim. Past*, 9, 871–886,  
424 doi:10.5194/cp-9-871-2013, 2013.

425 Comas-Bru, L., McDermott, F. and Werner, M. (2016): The effect of the East Atlantic pattern on the precipitation  $\delta^{18}\text{O}$ -  
426 NAO relationship in Europe, *Climate Dynamics*, doi: 10.1007/s00382-015-2950-1

427 Dansgaard, W., Johnsen, S.J.: A flow model and a time scale for the ice core from Camp Century, Greenland, *J. Glaciol.*,  
428 8(53), 215–223, 1969.

429 Draxler, R.R., and Hess G.D.: An overview of the HYSPLIT\_4 modeling system of trajectories, dispersion, and deposition.  
430 *Aust. Meteor. Mag.*, 47, 295–308, 1998.

431 Ekaykin A.A., Lipenkov V.Ya.: Formation of the ice core isotopic composition, *Physics of ice core records II*, ed. T.Hondoh,  
432 *Low Temperature Science*, 68, Hokkaido Univ. Press, Sapporo, 299–314, 2009.

433 Elizbarashvili E.Sh., Elizbarashvili, M.R., Tatishvili, M.E., Elizbarashvili, Sh.E., Elizbarashvili, R.Sh.: Meskhiya Air  
434 temperature trends in Georgia under global warming conditions, *Russ. Meteorol. Hydrol.*, 38, 234–238, 2013.

435 Forster C., Stohl A., Siebert P.: Parametrization of convective transport in a lagrangian particle dispersion model and its  
436 evaluation, *Journ. of Applied Meteorology and Climatology*, 46 (4), 403–422, doi:10.1175/JAM2470.1, 2007.

437 Frew, R., Dennis, P.F., Heywood K.J., Meredith M.P., and Boswell S.M.: The oxygen isotope composition of water masses  
438 in the northern North Atlantic, *Deep Sea Research Part I: Oceanographic Research Papers*, 47, 12, 2265–2286,  
439 doi:10.1016/S0967-0637(00)00023-6, 2000.

440 Gat, J.R., Shemesh, A., Tziperman, E., Hecht, A., Georgopoulos, D., and Basturk, O.: The stable isotope composition of  
441 waters of the eastern Mediterranean Sea, *J. Geophysical Res.*, 101, 3, 6441–6451, doi: 10.1029/95JC02829, 1996.



- 442 Johnsen S., Clausen H.B., Cuffey K.M., Hoffmann G., Schwander J., Creyts T.: Diffusion of stable isotopes in polar firn and  
443 ice: the isotope effect in firn diffusion, *Physics of Ice Core Records*, Edited by T. Hondoh, Hokkaido University Press,  
444 Sapporo, 121–140, 2000.
- 445 Kalnay, E., Kanamitsu, M., Kistler, R., Collins, W., Deaven, D., Gandin, L., Iredell, M., Saha, S., White, G., Woollen, J.,  
446 Zhu, Y., Leetmaa, A., Reynolds, B., Chelliah, M., Ebisuzaki, W., Higgins, W., Janowiak, J., Mo, K. C., Ropelewski, C.,  
447 Wang, J., Jenne, R., Joseph, D.: The NCEP/NCAR 40-Year Reanalysis Project, *Bulletin of the American Meteorological*  
448 *Society*, 77, 3, 437–472, doi: 10.1175/1520-0477(1996)077<0437:TNYRP>2.0.CO;2, 1996.
- 449 Kozachek A.V., Ekaykin A.A., Mikhailenko V.N., Lipenkov V.Y., Kutuzov S.S.: Isotopic composition of ice cores obtained  
450 at the Elbrus Western Plateau, *Ice and Snow*, 55, 4, doi: 10.15356/2076-6734-2015-4-35-49, 35-49, 2015 (in Russian with  
451 English summary)
- 452 Kutuzov, S., Shahgedanova, M., Mikhailenko, V., Lavrentiev, I., and Kemp, S.: Desert dust deposition on Mt. Elbrus,  
453 Caucasus Mountains, Russia in 2009–2012 as recorded in snow and shallow ice core: high-resolution “provenancing”,  
454 transport patterns, physical properties and soluble ionic composition, *The Cryosphere*, 7(5), 1481–1498, doi:10.5194/tc-7-  
455 1481-2013, 2013.
- 456 Langebroek, P. M.; Werner, M.; Lohmann, G.: Climate information imprinted in oxygen-isotopic composition of  
457 precipitation in Europe, *Earth and Planetary Science Letters*, 311, 1, 144–154, 10.1016/j.epsl.2011.08.049, 2011.
- 458 Mariani I., Eichler A., Jenk M., Brönnimann S., Auchmann R., Leuenberger M.C., Schwikowski M.: Temperature and  
459 precipitation signal in two Alpine ice cores over the period 1961–2001, *Clim. Past*, 10, 1093–1108, doi:10.5194/cp-10-1093-  
460 2014, 2014.
- 461 Mikhailenko V., Sokratov S., Kutuzov S., Ginot P., Legrand M., Preunkert S., Lavrentiev I., Kozachek A., Ekaykin A., Faïn  
462 X., Lim S., Schotterer U., Lipenkov V., Toropov P.: Investigation of a deep ice core from the Elbrus western plateau, the  
463 Caucasus, Russia, *The Cryosphere*, 9, 2253–2270, doi:10.5194/tc-9-2253-2015, 2015.
- 464 Mikhailenko, V.N., Kuruzov, S.S., Lavrentiev, I.I., Kunakhovich, M.G., and Thompson, L.G.: Issledovanie zapadnogo  
465 lednikovogo plato Elbrusa: rezul'taty i perspektivy (Western Elbrus Plateau studies: results and perspectives), *Materialy*  
466 *glyatsiologicheskikh issledovaniy (Data Glaciol. Stud.)*, (99), 185–190, 2005 (in Russian with English summary)
- 467 Mountain Research Initiative EDW Working Group: Elevation-dependent warming in mountain regions of the world, *Nature*  
468 *Climate Change* 5, 424–430, doi:10.1038/nclimate2563, 2015.
- 469 Panagiotopoulos F., Shahgedanova M., Steffenson D.B.: A review of Northern Hemisphere winter time teleconnection  
470 patterns, *J. Phys. IV France*, 12, doi: 10.1051/jp4:20020450, 2002.
- 471 Pfahl S. and Wernli H.: Air parcel trajectory analysis of stable isotopes in water vapor in the eastern Mediterranean, *J.*  
472 *Geophys. Res.*, 113, D20104, doi:10.1029/2008JD009839, 2008.
- 473 Risi C., Bony S., Vimeux F., Jouzel J.: Water stable isotopes in the LMDZ4 general circulation model: Model evaluation for  
474 present-day and past climate and implications to climatic interpretation of tropical isotopic records, *Journal of Geophysical*  
475 *Research*, 115, D12118, doi:10.1029/2009JD013255, 2010.

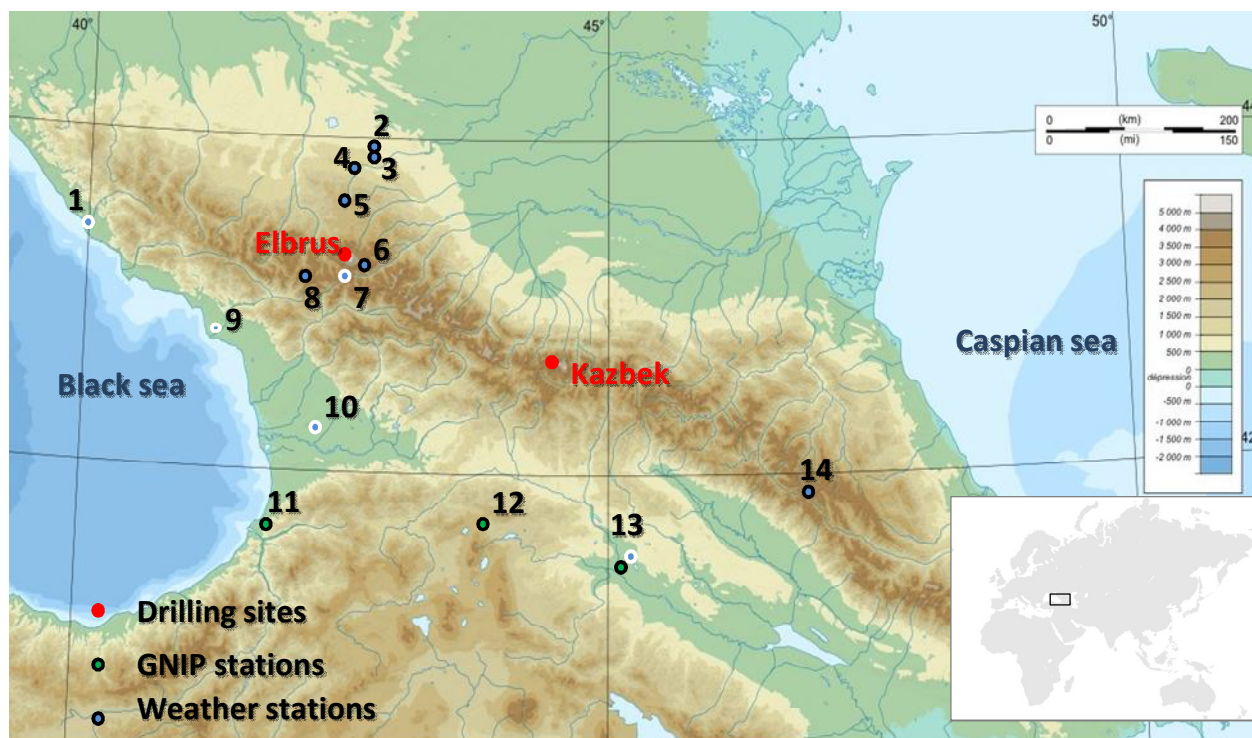




- 476 Rolph, G.D., Real-time Environmental Applications and Display sYstem (READY) Website (<http://ready.arl.noaa.gov>).  
477 NOAA Air Resources Laboratory, Silver Spring, MD, 2016.
- 478 Shahgedanova M., Nosenko G., Kutuzov S., Rototaeva O., and Khromova T.: Deglaciation of the Caucasus Mountains,  
479 Russia/Georgia, in the 21st century observed with ASTER satellite imagery and aerial photography, *The Cryosphere*, 8(6),  
480 2367–2379, doi:10.5194/tc-8-2367-2014, 2014.
- 481 Shahgedanova M., Stokes C., Gurney S., Popovnin V.: Interactions between mass balance, atmospheric circulation, and  
482 recent climate change on the Djankuat Glacier, Caucasus Mountains, Russia, *Journ. of Geophys. Research*, 110, D04108,  
483 doi:10.1029/2004JD005213, 2005.
- 484 Stein, A.F., Draxler, R.R., Rolph, G.D., Stunder, B.J.B., Cohen, M.D., and Ngan, F.: NOAA's HYSPLIT atmospheric  
485 transport and dispersion modeling system, *Bull. Amer. Meteor. Soc.*, 96, 2059–2077, doi: 10.1175/BAMS-D-14-00110.1,  
486 2015.
- 487 Stoffel M., Khodri M., Corona C., Guillet S., Poulain V., Bekki S., Guiot J., Luckman B.H., Oppenheimer C., Lebas N.,  
488 Beniston M., and Masson-Delmotte V.: Estimates of volcanic-induced cooling in the Northern Hemisphere over the past  
489 1,500 years, *Nature Geoscience* 8, 784–788, doi:10.1038/ngeo2526, 2015.
- 490 Stohl A., Thompson D.J.: A density correction for lagrangian particle dispersion models, *Boundary Layer Meteorology*, 90  
491 (1), 155–167, doi:10.1023/A:1001741110696, 1999.
- 492 Tielidze L.G.: Glacier change over the last century, Caucasus Mountains, Georgia, observed from old topographical maps,  
493 Landsat and ASTER satellite imagery, *The Cryosphere*, 10, 713–725, doi:10.5194/tc-10-713-2016, 2016.
- 494 Toropov P.A., Mikhailenko V.N., Kutuzov S.S., Morozova P.A., Shestakova A.A.: Temperature and radiation regime of  
495 glaciers on slopes of the Mount Elbrus in the ablation period over last 65 years, *Ice and Snow*, 56(1), 5–19,  
496 doi:10.15356/2076-6734-2016-1-5-19, 2016 (In Russian with English summary).
- 497 Tsushima A., Matoba S., Shiraiwa T., Okamoto S., Sasaki H., Solie D.J., Yoshikawa K.: Reconstruction of recent climate  
498 change in Alaska from the Aurora Peak ice core, central Alaska, *Clim. Past*, 11, 217–226, doi:10.5194/cp-11-217-2015,  
499 2015.
- 500 Vladimirova D.O. and Ekaykin A.A.: Climatic variability in Davis Sea sector (East Antarctica) over the past 250 years based  
501 on the 105 km ice core geochemical data, *Problemy Arktiki i Antarktiki*, 1 (99), 102–113, 2014. (In Russian with English  
502 summary).
- 503 Volodicheva, N.: The Caucasus, in: *The Physical geography of Northern Eurasia*, edited by: Shahgedanova, M., Oxford  
504 University Press, Oxford, 350–376, 2002
- 505 Wagenbach, D., Bohleber, P. and Preunkert, S.: Cold alpine ice bodies revisited: what may we learn from their impurity and  
506 isotope content? *Geografiska Annaler: Series A, Physical Geography*, 94, 245–263. doi:10.1111/j.1468-0459.2012.00461.x,  
507 2012.

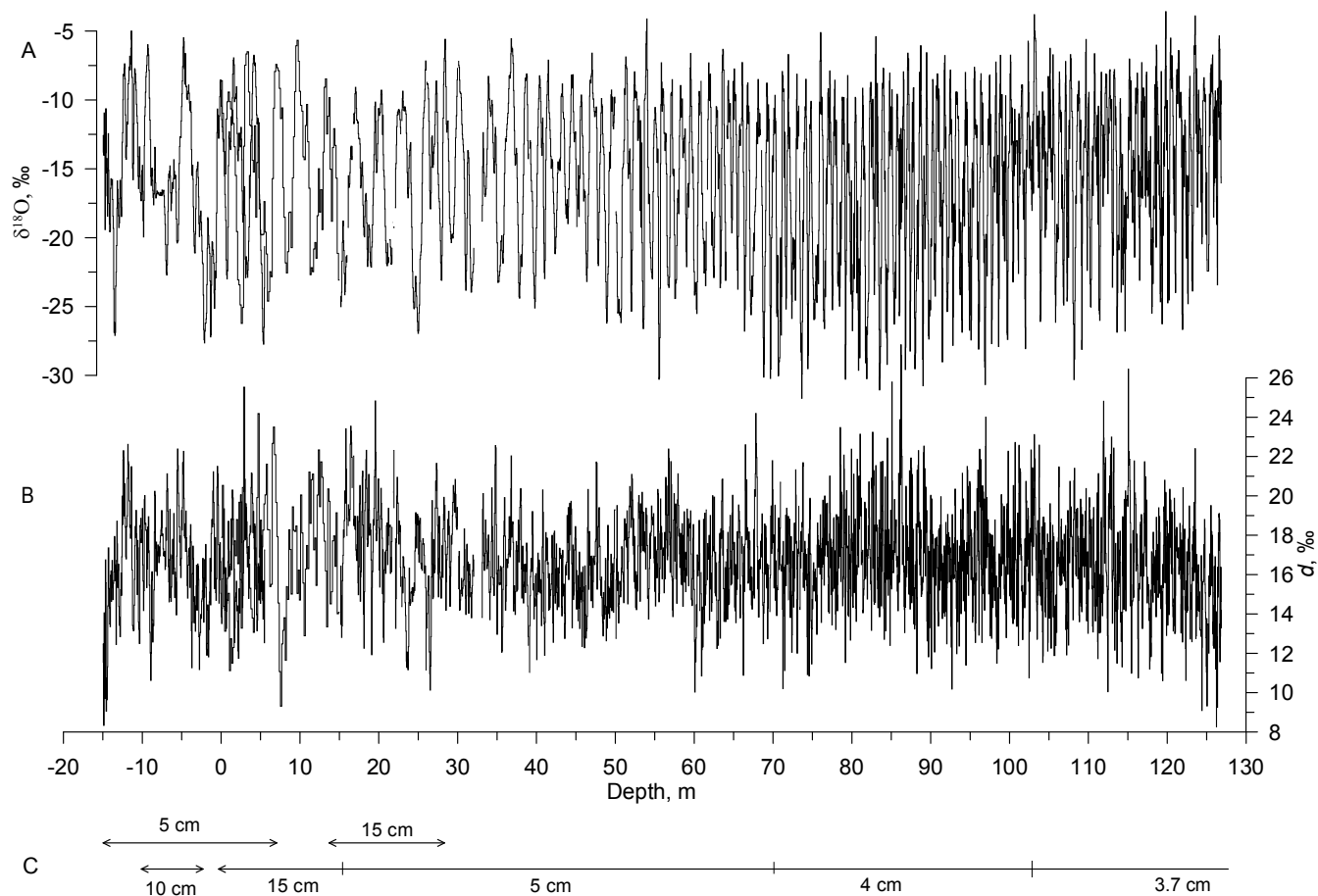


508  
509  
Figures



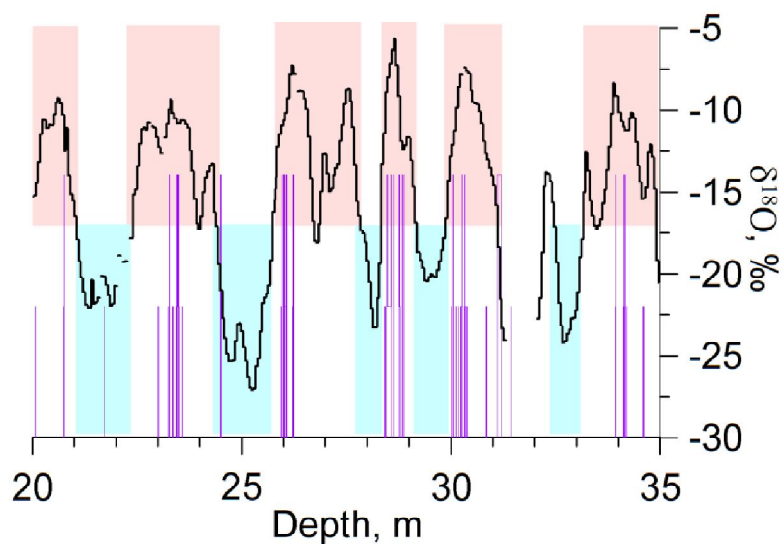
510  
511  
512  
513  
514  
515  
516  
517  
518

Fig. 1: Map showing the region around Elbrus (black rectangle in the world's map in the lower right corner), with shading indicating elevation (m above sea level). Drilling sites are indicated with red filled circles, GNIP stations as green filled circles, and meteorological stations as blue dots. Stations situated to the south of the Main Caucasus Ridge according to the precipitation cycle pattern are shown using a blue dot with white outside circle and the stations situated to the north are displayed with black outside circle (see text for the details). The number of the various stations refers to Table 1 for their detailed description.



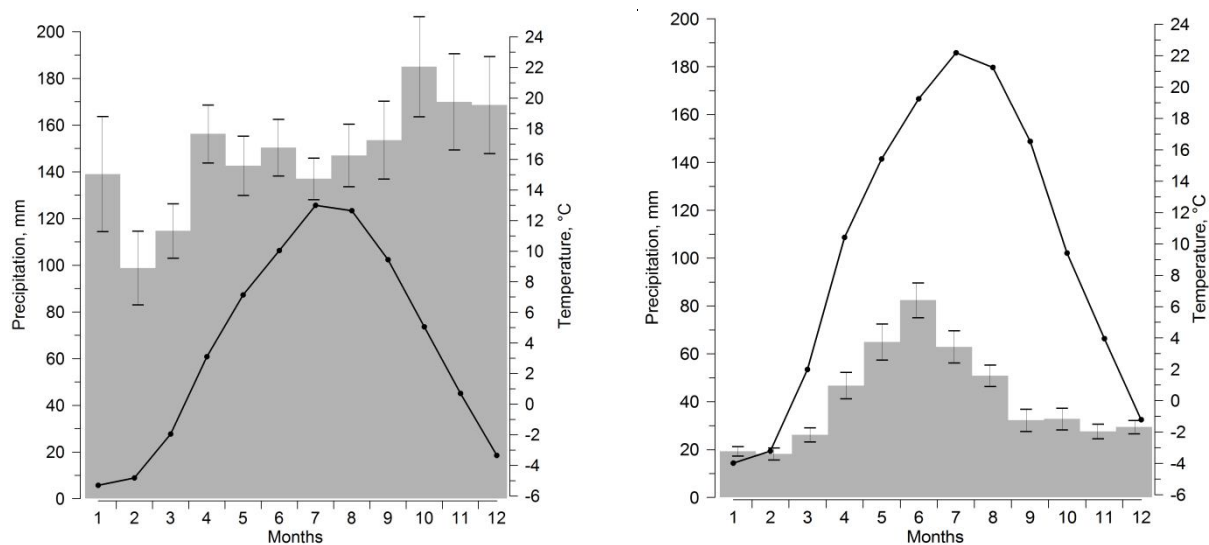
**Fig. 2.** Vertical profile of  $\delta^{18}\text{O}$  (A), deuterium excess (B), and the number of the ice core as well as sampling resolution (C). 0 m depth corresponds to the surface of 2009.

519  
520  
521  
522  
523



524  
525  
526  
527  
528

**Fig. 3:** Illustration of the scheme used to identify warm and cold half-years (respectively indicated by the light red and light blue shaded areas) based on the deviation of the mean  $\delta^{18}\text{O}$  values from the long-term average value. The purple lines depict the melt layers observed in the core.



529  
530  
531  
532  
533  
534  
535  
536

**Fig. 4: Average seasonal cycle of temperature (black dots and line) and precipitation (grey bars) calculated over 1966-1990 period, a) for the Klukhorskyy Pereval station (illustrating the lack of a distinct seasonal cycle in precipitation south of the Caucasus) and b) for the Mineralnye Vody station (illustrating the clear seasonal cycle in precipitation seen in stations north of the Caucasus). Error bars (SEM) are shown for the interannual standard deviation of the monthly precipitation rate while the same error bars for the temperature are dimensionless at the scale of the graph.**

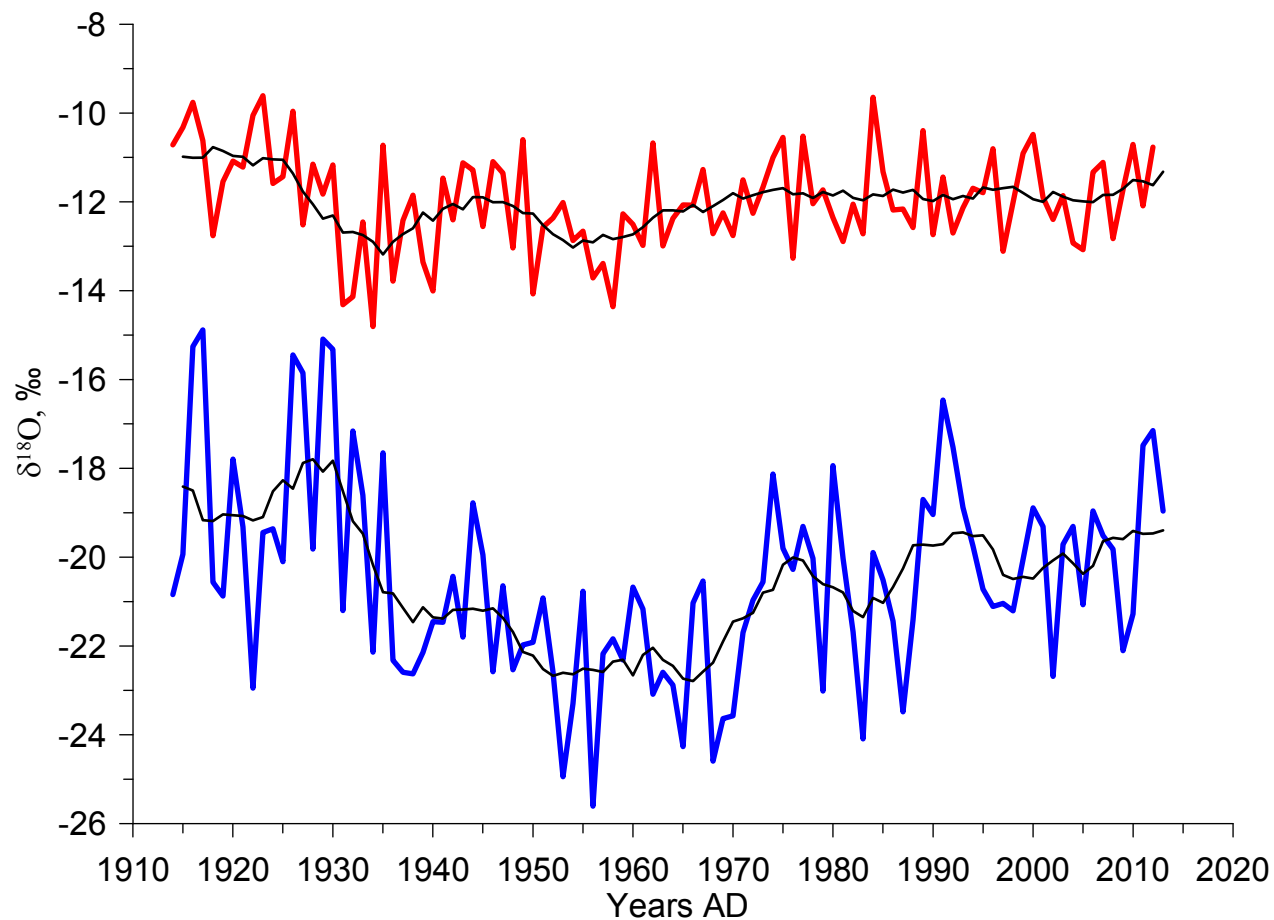


Fig. 5: Annual variations of  $\delta^{18}\text{O}$  in summer (red line) and in winter (blue line). Thin black lines show 10-year running means of these parameters.

537  
538  
539  
540



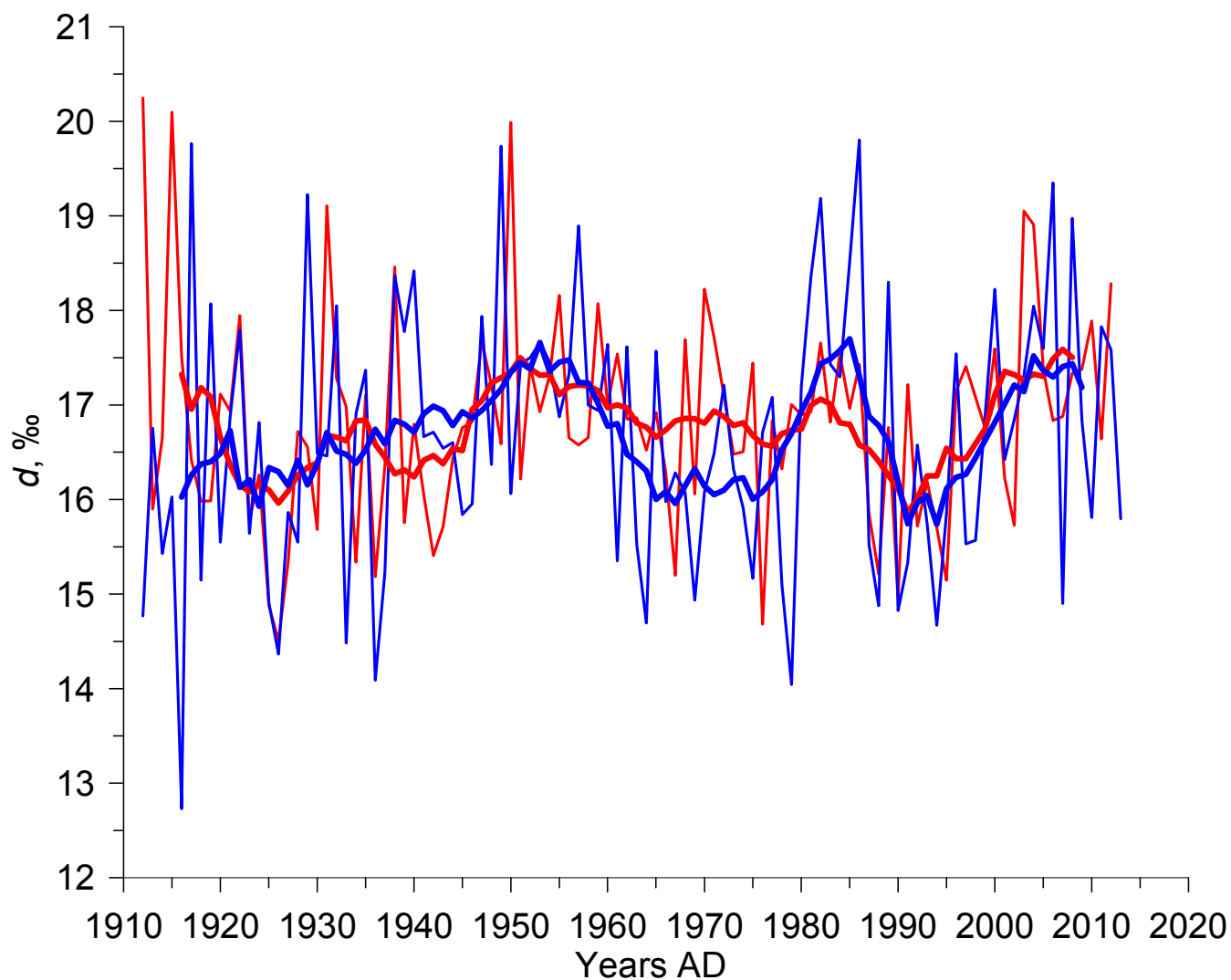
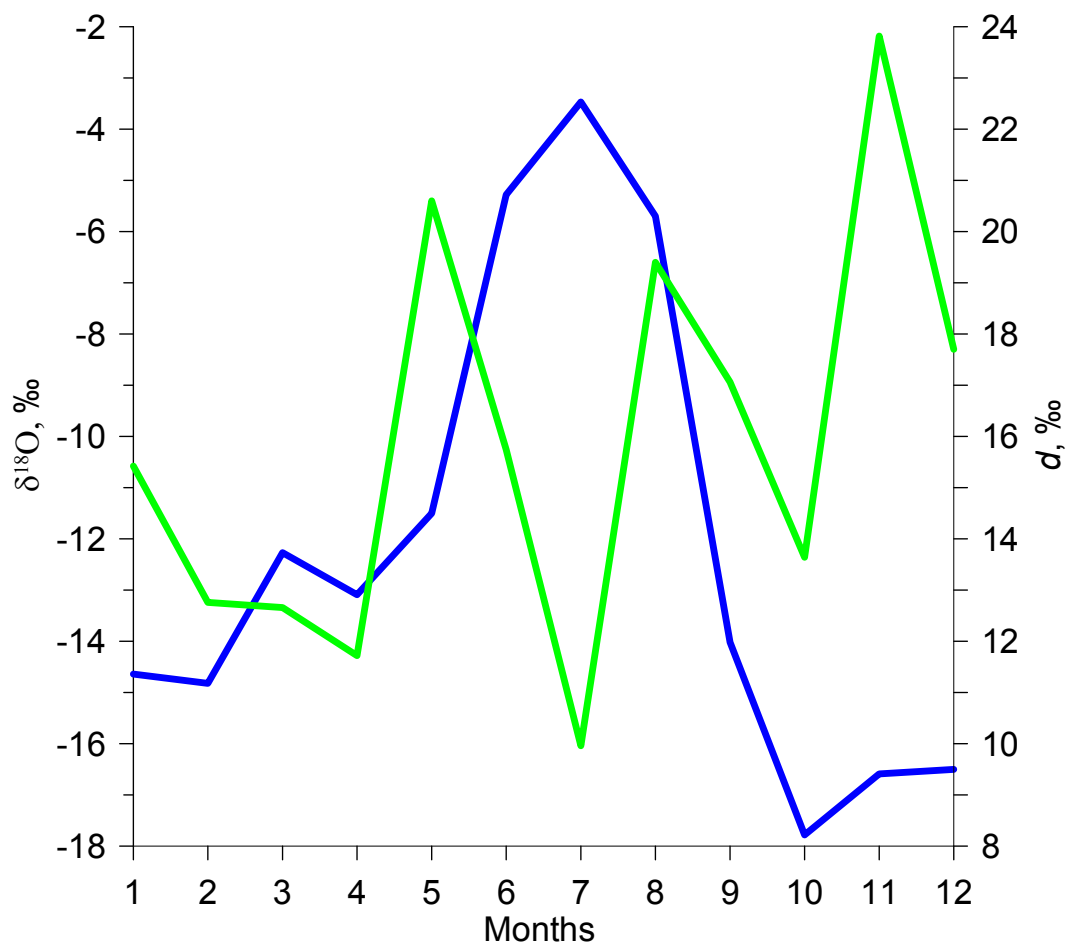


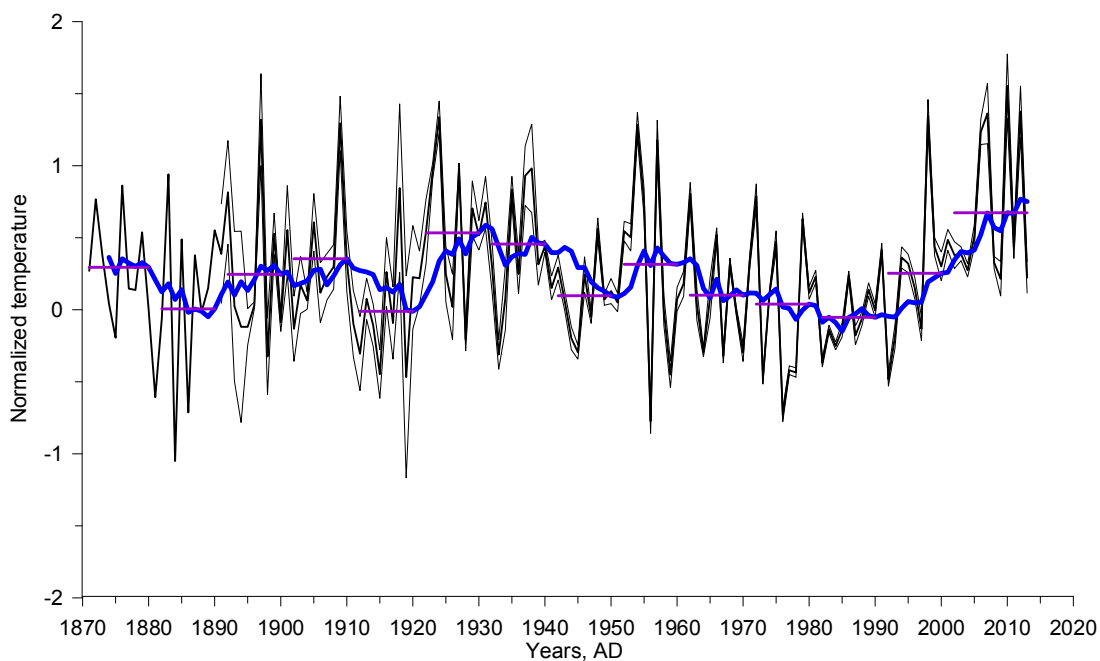
Fig. 6: Annual variations of deuterium excess in summer (red line) and in winter (blue line). Thick lines show the 10-year smoothed values and the thin ones display the raw values.

541  
542  
543  
544

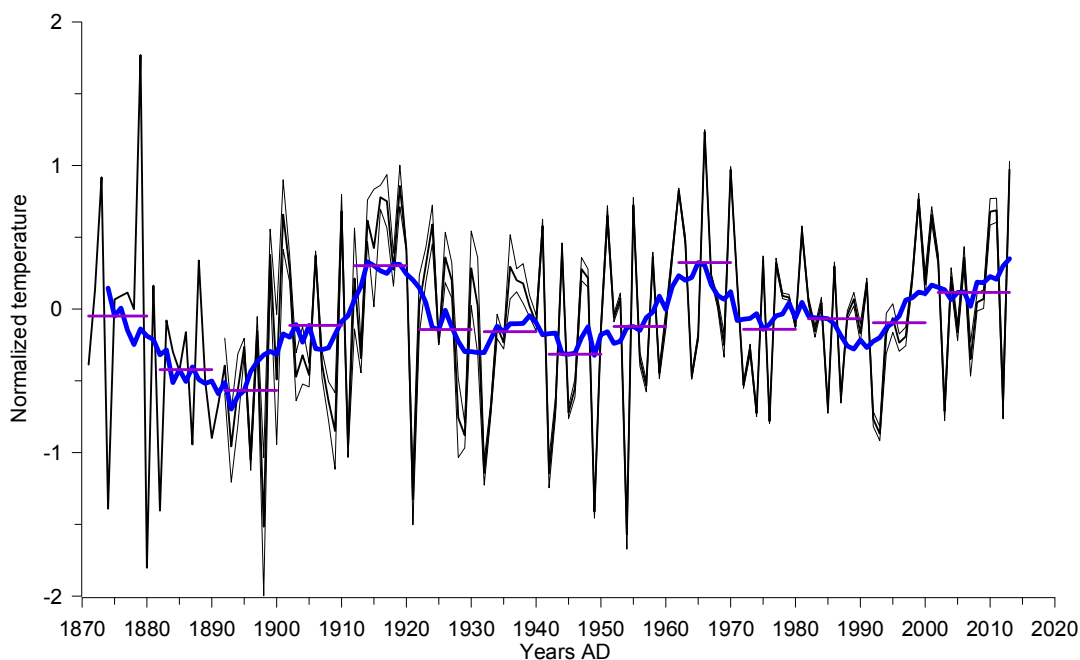


545  
546  
547  
548  
549  
550

Fig. 7: Monthly  $\delta^{18}\text{O}$  (blue line) and  $d$  (green line) data at Bakuriani GNIP station in 2009 (see Table 1 for information on station and Fig. 1 for its location). Note that there is no clear seasonal cycle in deuterium excess, in contrast with  $\delta^{18}\text{O}$  showing maximum values in summer and minimum values in winter.

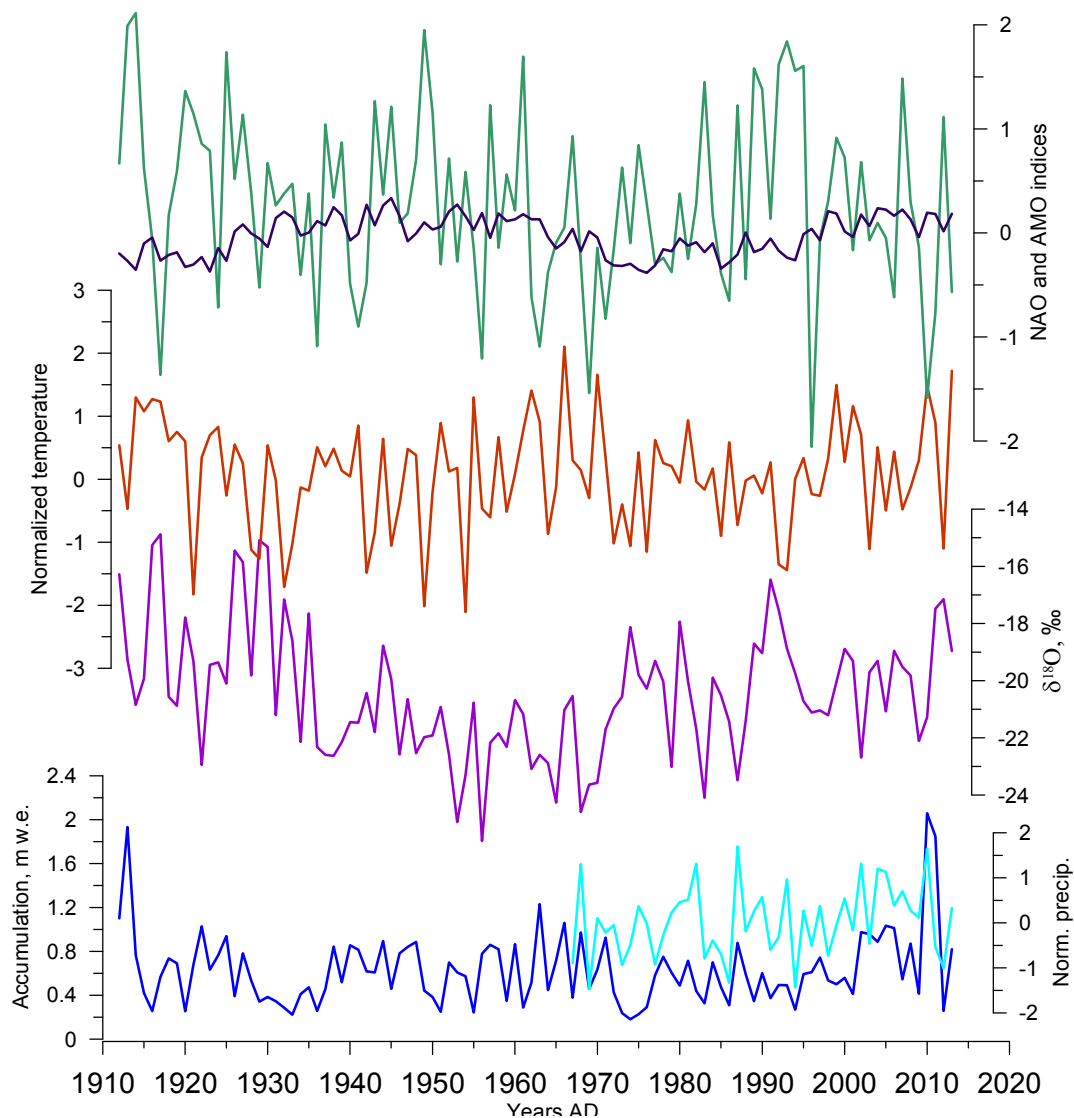


551  
552



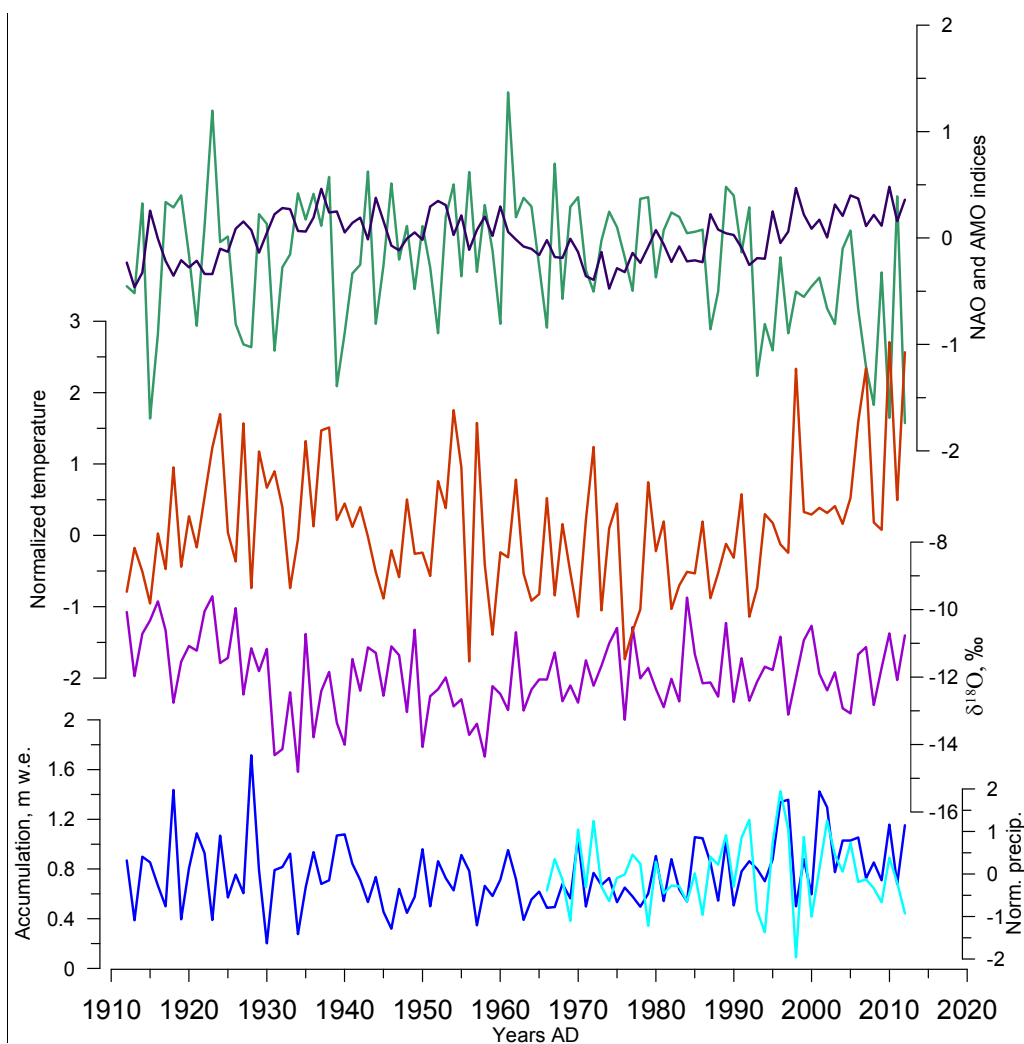
553  
554  
555  
556  
557  
558  
559  
560

**Fig. 8: Normalized regional temperature record based on meteorological data, with respect to the reference period 1966-1990, expressed as annual anomalies (°C). The thin lines illustrate the standard deviation across the individual records after accounting for the lapse rate from Fig. S3, the blue line shows 10 year running mean and the horizontal purple line demonstrates the decadal mean value, the upper panel for the warm season, and the lower panel for the cold season.**

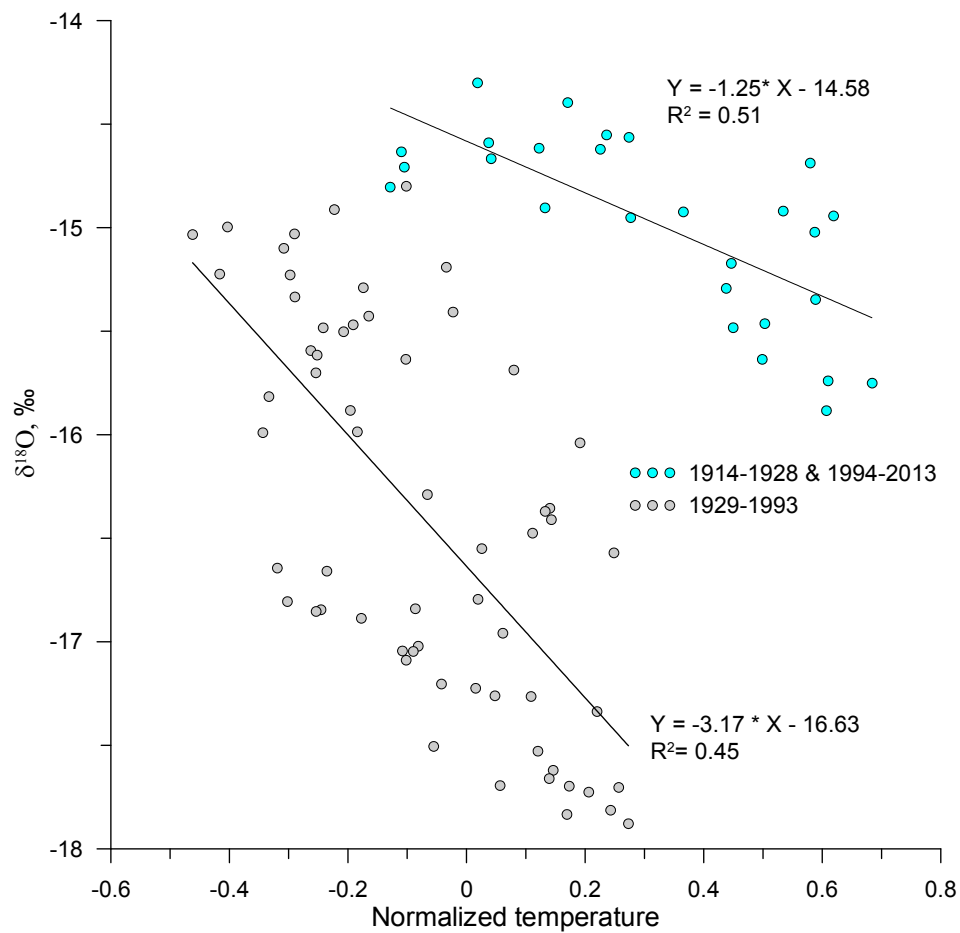


561  
562  
563  
564  
565  
566

**Fig. 9:** Comparison of the ice core record with instrumental regional climate information, for the cold season:  $\delta^{18}\text{O}$  composite (purple), regional meteorological composites of temperature (brown), precipitation to the south from the Caucasus (light blue) as well as the ice core accumulation estimate (dark blue) and NAO (green) and AMO (dark) indices.



567  
568  
569  
570  
571  
572  
Fig. 10: Comparison of the ice core record with instrumental regional climate information, for the warm season:  $\delta^{18}\text{O}$  composite (purple), regional meteorological composites of temperature (brown), precipitation to the south from the Caucasus (light blue) as well as the ice core accumulation estimate (dark blue) and NAO (green) and AMO (dark) indices.



573  
574  
575

Fig. 11. Correlation plot and regression lines for the 11-year running means of the annual local temperature and annual  $\delta^{18}\text{O}$ .



576 **Table 1: Description of meteorological and instrumental data used in the paper**

Data type	Number on map (Fig. 1)	Location/Name	Altitude a.s.l.	Time span	Data source		
Meteorological observations (temperature, precipitation rate) with daily resolution	1	Sochi	57 m	1871-present	www.meteo.ru		
	2	Mineralnye Vody	315 m	1938-present			
	3	Kislovodsk	943 m	1940-present			
	4	Pyatigorsk	538 m	1891-1997			
	5	Shadzhatmaz	2070 m	1959-present			
	6	Terskol	2133 m	1951-2005			
	7	Klukhorskiy Pereval	2037 m	1959-present			
	8	Teberda	1550 m	1956-2005			
	9	Sukhumi	75 m	1904-1988			
	10	Samtredia	24 m	1936-1992			
	13	Tbilisi	448 m	1881-1992			
	14	Sulak	2927 m	1930-present			
	15	Mestia	1417 m	1930-1991			
	GNIP data	11	Batumi	32 m		1980-1990	<a href="http://www-naweb.iaea.org/napc/ih/IHS_resources_gnip.html">http://www-naweb.iaea.org/napc/ih/IHS_resources_gnip.html</a>
		12	Bakuriani	1700 m		2008-2009	
13		Tbilisi	448 m	2008-2009			
Circulation indices	n/a	NAO	n/a	1821-present	Vinter et al., 2009 <a href="https://crudata.uea.ac.uk/~timo/datasets/naoi.htm">https://crudata.uea.ac.uk/~timo/datasets/naoi.htm</a> <a href="http://www.cpc.ncep.noaa.gov/products/precip/CWlink/">http://www.cpc.ncep.noaa.gov/products/precip/CWlink/</a>		
			n/a	1950-present			
	n/a	NCP	n/a	1948-present			
	n/a	AO	n/a	1950-present			
	n/a	AMO	n/a	1856-present			
Reanalysis daily temperature	n/a	NCEP	500 mb level	1948-present	<a href="http://www.esrl.noaa.gov/psd/data/gridded/data.ncep.reanalysis.html">http://www.esrl.noaa.gov/psd/data/gridded/data.ncep.reanalysis.html</a> Kalnay et al., 1996		
Back trajectories	n/a	Flexpart	n/a	2002-2009	Forster et al., 2007, Stohl et al., 2009		
	n/a	Hysplit	n/a	1948-present	Draxler, 1999, Stein et al., 2015, Rolph, 2016		
	n/a	LMDZiso	n/a	n/a	Risi et al., 2010		

577



578  
579  
580

**Table 2: Correlation coefficients between meteorological data and indices of large-scale modes of variability (statistically significant coefficients at  $p < 0.05$  are highlighted in bold).**

	SUMMER			WINTER		
	Temperature	P south*	P north*	Temperature	P south*	P north*
NAO	<b>-0.47</b>	<b>0.23</b>	-0.03	<b>-0.41</b>	0.04	<b>0.26</b>
AO	-0.11	0.08	-0.14	<b>-0.40</b>	0.14	<b>0.37</b>
AMO	<b>0.24</b>	0.01	-0.02	0.07	<b>0.27</b>	<b>0.25</b>
NCP	<b>-0.50</b>	<b>0.34</b>	0.18	<b>-0.77</b>	<b>0.25</b>	<b>0.33</b>

581  
582  
583  
584

\*P south – precipitation rate at the weather stations to the South from the Caucasus, P north – precipitation rate at the weather stations to the North from the Caucasus.



585  
586

**Table 3: Mean characteristics of the Elbrus ice core records, calculated for the period from 1914 to 2013.**

<b>Winter</b>	$\delta^{18}\text{O}$ , ‰	$\delta\text{D}$ , ‰	$d$ , ‰	Accumulation rate (mm w.e./year)
Mean	-21.20	-152.42	17.16	0.61
Standard deviation	2.18	17.44	1.41	0.31
<b>Summer</b>				
Mean	-11.80	-77.32	17.06	0.76
Standard deviation	1.02	8.10	1.15	0.26

587  
588


 589  
 590  
 591

**Table 4. Correlation coefficients between ice core data, meteorological data and indices of large-scale modes of variability (statistically significant coefficients at  $p < 0.05$  are highlighted in bold).**

Summer	$\delta^{18}\text{O}$	Accumulation	$d$	NAO	AO	NCP
$T$ , °C	0.13	0.09	<b>0.21</b>	<b>-0.48</b>	-0.10	<b>-0.51</b>
P north	0.07	<b>0.24</b>	0.11	-0.03	-0.14	0.18
P south	-0.12	<b>0.44</b>	-0.04	0.23	0.08	0.34
$\delta^{18}\text{O}$		-0.17	-0.11	0.06	<b>0.23</b>	-0.04
Accumulation			<b>0.27</b>	<b>-0.25</b>	0.05	0.07
$d$				-0.17	0.00	<b>-0.18</b>
Winter	$\delta^{18}\text{O}$	Accumulation	$d$	NAO	AO	NCP
$T$ , °C	-0.02	<b>0.31</b>	-0.08	<b>-0.42</b>	<b>-0.45</b>	<b>-0.79</b>
P north	<b>0.25</b>	0.13	-0.01	<b>0.26</b>	<b>0.37</b>	<b>0.23</b>
P south	-0.09	<b>0.44</b>	-0.06	0.04	0.14	<b>0.25</b>
$\delta^{18}\text{O}$		-0.05	-0.04	<b>0.42</b>	<b>0.34</b>	0.08
Accumulation			0.04	<b>-0.34</b>	<b>-0.35</b>	0.05
$d$				0.05	-0.09	0.04

 592  
 593

\*P south – precipitation rate at the weather stations to the South from the Caucasus, P north – precipitation rate at the weather stations to the North from the Caucasus.